SUBSURFACE PROCESSES LAB

Fiber-Laden Proppant Placement in a Deformable Fracture:
Influence of Fracture-Surface Roughness

Ricardo Medina[1], Russell Detwiler[1], Romain Prioul[2], Wenyue Xu[2], J. Alberto Ortega[3]
[1]Civil and Environmental Engineering, University of California, Irvine; [2]Schlumberger-Doll Research, Cambridge, MA; [3]Schlumberger, Sugar Land, TX

UCI University of California, Irvine

Schlumberger

H41E-1369

Introduction

During the shut-in stage of hydraulic fracturing, aperture decreases and proppant is trapped between the fracture walls. The amount and distribution of the trapped proppant determines the fracture conductivity after fracture closure. Conventional fluids used in hydraulic fracturing typically form a uniform distribution of proppant within the fracture, i.e. proppant pack, and the fracture conductivity is control by the proppant pack permeability. In recent experiments, the addition of fibers to proppant mixtures has been shown to result in the formation of proppant-fiber regions surrounded by solids-free regions. The formation of such proppant-fiber regions has the potential to increase fracture permeability, however, the behavior of these islands when subjected to an applied stress is unknown. We present preliminary results from a series of experiments of fiber-proppant settling inside a deformable fracture with both smooth and rough walls. The proppant mixture was injected into the fracture and allowed to settle uninterrupted for twenty five minutes before we incrementally increased the load applied to the fracture surfaces from 0 to 90 kPa. The results for both smooth- and rough-walled fractures demonstrate the development of isolated proppant-fiber regions with some interconnected proppant-free regions. Our results suggest that in real fractures, in which surface roughness is non-negligible, the addition of fibers to proppant mixtures is likely to increase fracture conductivity relative to a similar proppant mixture without fibers.

Experimental setup: Transparent fracture with applied normal stress

Fig 1. Experimental setup. (a) Photograph of rotating sand (not shown: data acquisition system, outflow scale, filling tank, and electronic controllers). (b) Plan-view schematic of the fracture. (c) Schematic view of cross-section A-A′. (d) The smooth- and rough-walled fractures, each with mean aperture, ⟨b⟩.

The experimental system consists of a 15cm x 15cm fracture cell that allows the direct application of a normal stress to the fracture surfaces while the entire flow field is imaged using a high-resolution CCD camera. The stress is applied to the fracture through eight pneumatic actuators mounted on the fracture frame. Four LVDTs are securely mounted on the frame and record the fracture aperture reduction as the stress is increased. We compared the influence of surface roughness by repeating the experiment under the same conditions, but different fracture walls: smooth fracture (flat pieces of glass) and rough fracture (glass with a gauss-like pattern, b′ ≈150 μm) .

Experimental Procedure

The proppant mixture was prepared by adding 17.7% v/v of sand ($\phi_s = 0.177$) and 0.4% v/v of polymeric fibers ($\phi_f = 0.04$) to a shear-thinning viscous fluid (0.48% w/w guar-water, apparent viscosity of $\eta = 1.2$ Pa•s at a shear rate of $\dot{\gamma} = 0.1 s^{-1}$). The proppant mixture was injected into the fracture until ~10 fracture volumes had passed through the system. We allowed the proppant to settle uninterrupted for approximately 25 minutes. After the initial settling time we applied a normal stress at regular time intervals of ~50 minutes increasing by 12.8 kPa normal stress to a maximum of 88.9 kPa.

Converting transmitted light to solid volume fraction of sand (ϕ_s)

We use light transmission techniques to obtain accurate measurements of the fracture aperture field, b_{ij}. The Beer-Lambert law is used to calculate the absorbance field (A_{ij}) which is directly proportional to the aperture field (Detwiler, et al., 1999).

$$I = I_0 e^{-\mu C b}$$

$$A = ln\left(\frac{I_{clear}}{I_{dye}}\right) = \mu(C_d - C_c)b$$

$$b_{ij} = \frac{A}{\langle A \rangle}\langle b \rangle$$

A = Absorbance
b = Fracture aperture
C = Solute concentration
I = Measured light irradiance
I_0 = Source irradiance
μ = Solute attenuation coeff.
subscripts
d/c = dyed/clear water

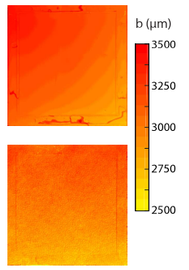

Fig 2. Measured fracture aperture field. Smooth-walled mean aperture, <b> = 3115 μm, RMS= 8 μm. Rough-walled mean aperture, <b> = 2982 μm, RMS = 62 μm.

The sand-fiber proppant images are processed using light transmission techniques. We derived a linear relationship between sand volume fraction (ϕ_s) and the measured absorbance (A), following the absorption and scattering theory described by Bohren and Huffman (1983).

$$A = \ln\left(\frac{I_{clear}}{I_{mix}}\right) = \ln\left(\frac{I_0 \exp^{(-\mu_{cf} b)}}{I_0 \exp^{(-\mu_{cf} b - n_s C_s b - n_f C_f b)}}\right)$$

$$= n_s A_{p,s} Q_s b + n_f A_{p,f} Q_f b$$

$$= \left(\frac{3\phi_s}{4\pi a^3}\right) A_{p,s} Q_s b + \left(\frac{4\phi_f}{\pi l d^2}\right) A_{p,f} Q_f b$$

$$= \phi_s \alpha_s b + \phi_f \alpha_f b$$

$$\boxed{\phi_s = \frac{A/b - \phi_f \alpha_f}{\alpha_s}}$$

A_p = Particle cross section
C = Extinction cross section
n = number particles/unit vol.
Q = Light extinction efficiency
a = Sand particle radius
l = Fiber length
d = Fiber diameter
α = Light abs./unit length
ϕ = Solid volume fraction
subscripts
s/f = sand/fiber

The light absorbance of sand (α_s) was measured independently in a separate settling experiment without fibers (Medina, et al. 2015, 2016). The light absorbance of fibers (α_f) was estimated by assuming both sand and fiber particles have the same extinction efficiency ($Q_s = Q_f$), which is a reasonable assumption when the particles are large compared to the incident light wavelength (Bohren and Huffman, 1983).

Uncertainty analysis

We performed an uncertainty analysis of our method to calculate the level of uncertainty of our estimated ϕ_s. Using the equation above and following the uncertainty propagation outlined by Taylor (1997), we can represent the relative uncertainty of the solid volume fraction as:

$$\frac{\delta\phi_s}{\phi_s} = \left[\left(\frac{A/b}{A/b - \phi_f\alpha_f}\right)^2 \left(\left(\frac{\delta A}{A}\right)^2 + \left(\frac{\delta b}{b}\right)^2\right) + \left(\frac{\phi_f\alpha_f}{A/b - \phi_f\alpha_f}\right)^2 \left(\left(\frac{\delta\phi_f}{\phi_f}\right)^2 + \left(\frac{\delta\alpha_f}{\alpha_f}\right)^2\right) + \left(\frac{\delta\alpha_s}{\alpha_s}\right)^2\right]^{1/2}$$

$\frac{\delta b}{b} = 0.0095$
$\frac{\delta A}{A} = 0.0138$
$\frac{\delta\phi_f}{\phi_f} = 0.0526$
$\frac{\delta\alpha_s}{\alpha_s} = 0.0520$
$\frac{\delta\alpha_f}{\alpha_f} = 0.1252$

where
δx = uncertainty of x
$\frac{\delta x}{x}$ = relative unc. of x

Based on our measured and estimated relative uncertainties, we estimate the relative uncertainty of ϕ_s to be approximately 0.055.

Experimental results: Fracture closure and ϕ_s-fields

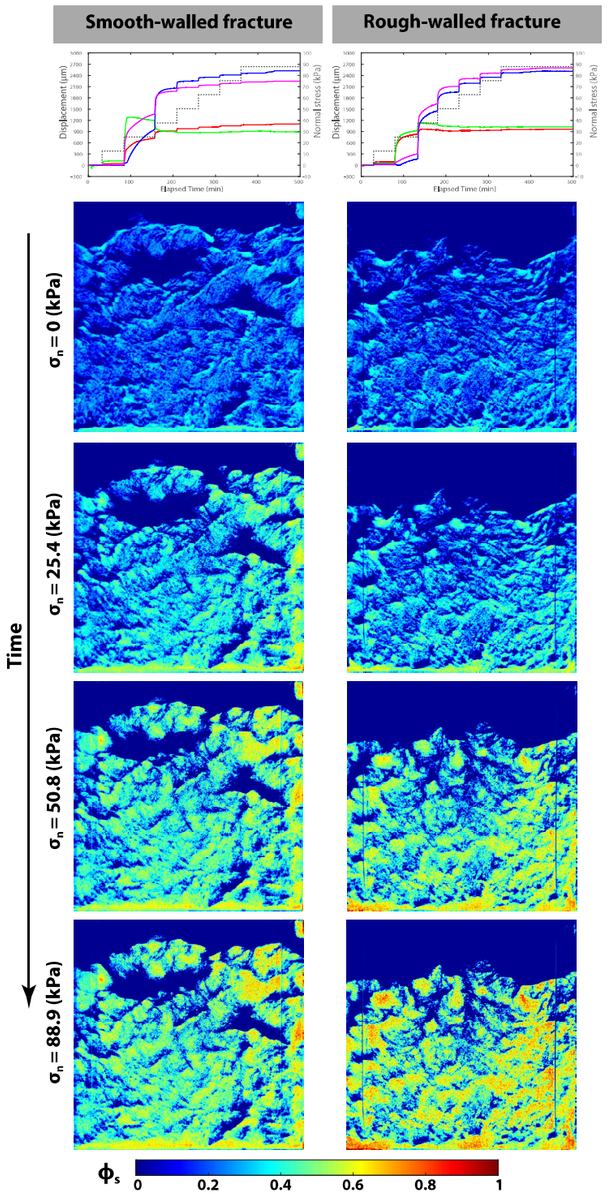

Fig 3. (Top) Measured displacement data for all LVDTs for both experiments. The color of the lines represent the different LVDT locations as indicated in Fig.1b. with the dashed line denoting the applied stress. (Bottom) Solid volume fraction distribution for the smooth-walled (left) and rough-walled (right) experiment. Both experiments were allowed to settle for ~25 minutes before the normal stress was applied; after that, we increased the applied normal stress in regular increments of 12.8 kPa up to a maximum normal stress of 88.9 kPa every ~50 minutes.

Load-bearing regions

We validated our method to calculate ϕ_s by performing a mass-balance of the total solids inside the fracture. In the smooth-walled experiment there is approximately 10.5 cm³ of sand, while in the rough walled fracture there were approx. 8.6 cm³ of sand (shown in Fig 4). The difference in total volume of sand is due to the difference in initial mean aperture $\Delta\langle b \rangle$ = 130 μm, which reduced the initial volume by 3.0 cm³. Error bars indicate the upper and lower bounds based on our error analysis.

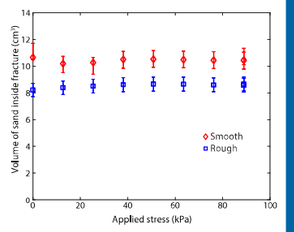

Fig 4. Total volume of sand inside the fractures. The difference corresponds to the difference in initial fracture volume and possible difference in initial filling state.

We identified the regions of sand between the fracture walls supporting the applied stress (i.e. load-bearing regions). These regions prevent the fracture from closing as the stress increases, and are defined here as those regions with $\phi_s > 0.55$, which is the minimum solid volume fraction required for the particles to come into contact (Onoda & Liniger, 1990). We calculated the total area and distribution of the load bearing sand. Of all the regions with some solids, only a small fraction of these regions are actually carrying the load (Fig. 5a). The load was transferred from the manifolds to the sand after $\sigma_n > 25.4$ kPa and the area covered by these load-bearing regions increased linearly with increased stress. The linear increase in total area suggest the regions are spreading and compacting at the same time.

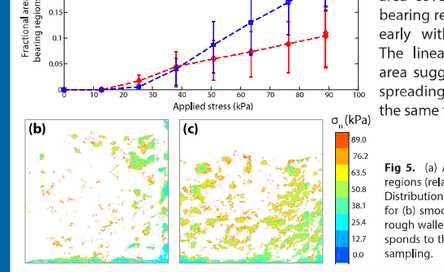

Fig 5. (a) Area of total load-bearing regions (relative to total fracture area). Distribution of load-bearing regions for (b) smooth walled fracture and (c) rough walled fracture. The color corresponds to the given time (or stress) of sampling.

Conclusions

- We applied a stress to a transparent fracture and quantified the behavior and concentrations of solids inside the fracture.
- We developed a method to calculate the solid volume fraction distribution of sand settling inside the transparent fracture.
- Roughness on the fracture led to more evenly distributed regions and increased the total area covered by load-bearing regions.
- The favorable distribution of 'load-bearing' regions indicates that the use of fibers might help in the creation of conductive channels within the fracture

References

Bohren, C.F. & Huffman, D.R. Absorption and scattering of light by small particles. Wiley, New York, 1983.
Detwiler, et al. *Water Res. Research*. 1999, **35**(9) 2605-2617.
Medina, et al. *Geofluids*. 2015, **15**(1-2) 24-36
Medina, et al. *American Rock Mechanics Association*. 2016
Onoda, G.Y. & Liniger, E.G. Phys Rev. Lett. 1990, **64**(22) 2727-2730.
Taylor, J.R. An Introduction to error analysis, the study of uncertainties in physical measurements. University Science Books, California, 1997.